Support information

Strongly coupled Ag/Cu with MXene for efficient tandem nitrate reduction reaction and zinc-nitrate battery

Bin Kui,[‡a] Shuang Zhao,[‡a] Yunhong Hu,[‡b] Kai Zheng,[a] Yuanhui Yao,[a] Song Chen,[c] Nana Wang,[d] Peng Gao,*[a] Zhongchao Bai,*[e] and Wei Ye*[a]

a. College of Material, Chemistry and Chemical Engineering, Key Laboratory of Organosilicon Chemistry and Material Technology, Ministry of Education, Hangzhou Normal University, Hangzhou, Zhejiang, 311121, China.

b. State Key Laboratory of Biocatalysis and Enzyme Engineering, School of Life Sciences, Hubei University, 430062, China.

c. Kharkiv Institute, Hangzhou Normal University, Hangzhou 311121, China.

d. Institute for Superconducting and Electronic Materials (ISEM), Innovation Campus, University of Wollongong, Squires Way, North Wollongong NSW 2500, Australia.

e. Institute of Energy Materials Science (IEMS), University of Shanghai for Science and Technology, Shanghai 200093, China.

*Corresponding author:

Peng Gao, E-mail: gaopeng@hznu.edu.cn.

Zhongchao Bai, E-mail: baizhongchao@tyut.edu.cn.

Wei Ye, E-mail: yewei@hznu.edu.cn.

Experimental procedures

Chemicals.

Silver nitrate ($AgNO_3$, A.R.), copper(II) chloride dihydrate ($CuCl_2{\cdot}2H_2O$, A.R.), sodium borohydride ($NaBH_4$, A.R.), sodium salicylate ($NaC_7H_5O_3$, A.R.), sodium citrate ($Na_3C_6H_5O_7$, A.R.), Monopotassium monosodium tartrate tetrahydrate ($KNaC_4H_{12}O_{10}$, A.R.), sodium hydroxide (NaOH, A.R.), sodium hypochlorite (NaClO, A.R.), sodium nitroprusside ($FeNa_2C_5H_4N_6O_3$, A.R.), ammonium chloride (NH_4Cl, A.R.), sodium nitrite ($NaNO_2$, A.R.), ethanol (EtOH, A.R.), ^{15}N-labeled potassium nitrate ($K_{15}NO_3$, ≥99.5%), potassium nitrate (KNO_3, A.R.), ethylene glycol ($C_2H_6O_2$, A.R.), potassium hydroxide (KOH, A.R.), hydrochloric acid (HCl, A.R.), Lithium fluoride (LiF, A.R.), ultra-high purity Ar (99.999%) and Griess reagent were purchased from Sinopharm Chemical Reagent Co. Ltd. (Shanghai, China). Ti_3AlC_2 (400 mesh) was purchased from 11 tech. All chemicals were used without further purification. All aqueous solutions were prepared using de-ionized (DI) water with a resistivity of 18.25 $M\Omega{\cdot}cm^{-1}$.

Sample characterizations

Prior to electron microscopy characterizations, a drop of the suspension of nanostructures in ethanol was placed on a piece of carbon-coated copper grid and dried under ambient conditions. Transmission electron microscopy (TEM) and high-resolution TEM (HRTEM) images with the corresponding energy-dispersive X-ray spectroscopy (EDS) mapping profiles were collected on a JEOL JEM-2100F field-emission high-resolution transmission electron microscope operated at 200 kV. Powder X-ray diffraction (XRD) patterns were recorded on a Philips X'Pert Pro Super X-ray diffractometer with Cu-Kα radiation (λ = 1.5418 Å). X-ray photoelectron spectra (XPS) were collected on an ESCALab 250 X-ray photoelectron spectrometer with non-monochromatized Al-Kα X-rays as the excitation source.

Determination of ammonia (NH_3)

Indophenol assays method. Sodium salicylate (5 g) and Seignette salt (5 g) were dissolved in NaOH solution (100 mL, 1 M) to obtain solution A. NaClO (3.5 mL, 10% ~15%) was diluted with 96.5 mL DI water to obtain solution B. Sodium nitroferricyanide (0.2 g) was dissolved in 20 mL DI water to obtain solution C. To quantify NH_3, solution A, solution B, and solution C were added in turn in the diluted electrolyte solution (2 mL). After 2 h in a dark room at room temperature, its absorbance at 655 nm was acquired from the UV-Vis absorption spectrum. A series of standard NH_3 solutions were used to obtain the working curve for NH_3 determination.

Nesslar reagent method. Typically, the diluted electrolyte solution (5 mL) was added into seignette salt solution (100μL, 0.2M) to wipe off the possible metal cations contamination. Commercial Nessler reagent (150μL) was added into the above mixture for 10min. Absorbance at 420 nm was acquired from the UV-Vis absorption spectrum. A series of standard NH_3 solutions were used to obtain working curve for NH_3 determination.

Determination of nitrite ions (NO_2^-)

The nitrite ions were spectrophotometrically quantified with Griess reagent. Typically, Griess reagent (200 μL) was added into the electrolyte solution (5 mL). Then, the solution was heated to 100 °C and maintained at that temperature for 1 min. After it was cooled to room temperature, its UV-Vis absorption spectrum was acquired and the absorbance at 524 nm was obtained. A series of standard NO_2^- solutions were used to obtain the working curve for NO_2^- determination.

Determination of N_2, H_2

The amounts of H_2 and N_2 were quantified by a gas chromatograph (GC) equipped with thermal conductivity (TCD) detector.

The FEs for NO_2^-, NH_3, N_2, and H_2 were calculated according to Equations (2-5):

$$FE_{NO_2^-} = (2F \times C_{NO_2^-} \times V)/ (47 \times Q) \quad (2)$$

$$FE_{NH_3} = (8F \times C_{NH_3} \times V)/ (17 \times Q) \quad (3)$$

$$FE_{N_2} = (10F \times V/V_m)/ Q \quad (4)$$

$$FE_{H_2} = (2F \times V/V_m)/ Q \quad (5)$$

Where F is the Faraday constant (96485.3 C mol–1), C is the concentration, V is the volume, Vm is standard molar volume and Q is the total charge passed through the working electrode.

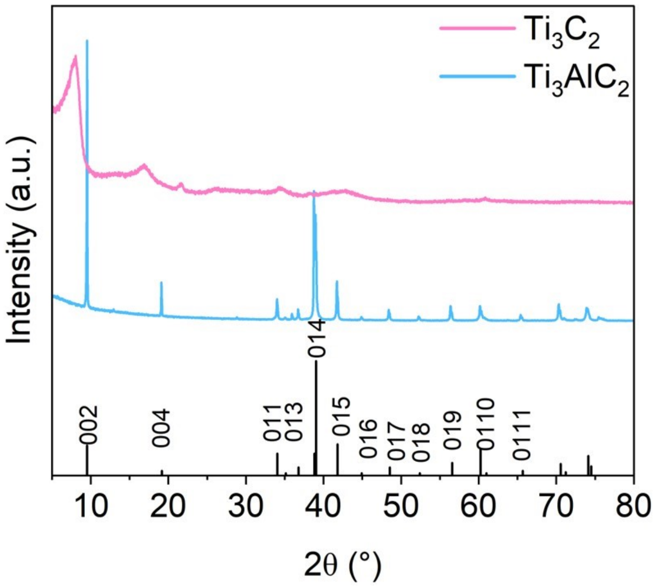

Fig. S1. XRD patterns of MXene and Ti_3AlC_2 MAX phase.

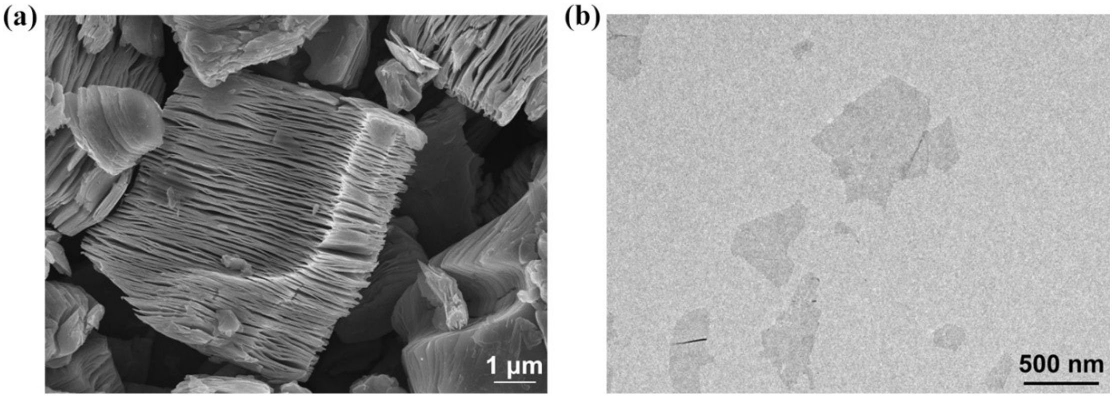

Fig. S2. (a) SEM image of multilayer MXene and (b) TEM image of the stripped MXene NSs.

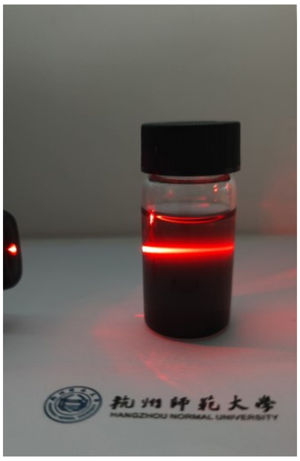

Fig. S3. The typical Tyndall effect of $Ti_3C_2T_x$ NSs solution.

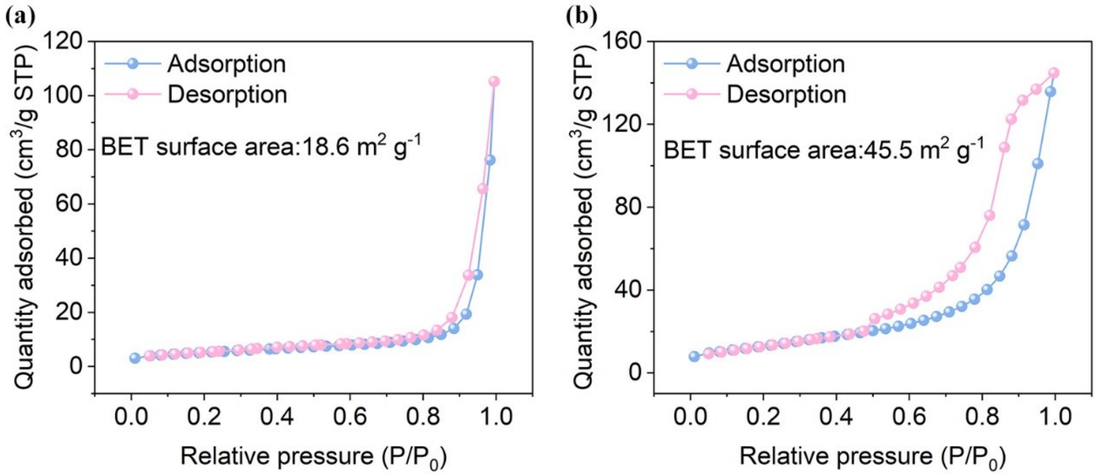

Fig. S4. N_2 adsorption and desorption isotherms of (a) the unstripped $Ti_3C_2T_x$ and (b) the stripped MXene.

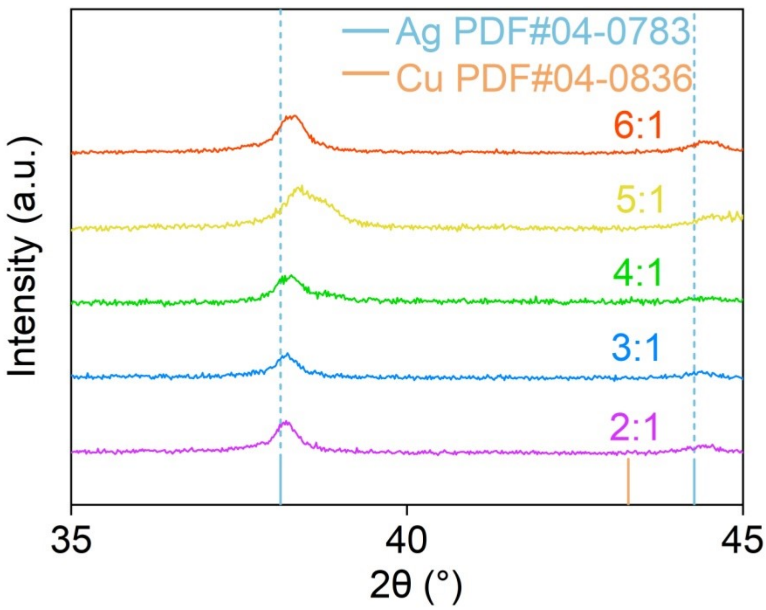

Fig. S5. The amplified XRD patterns of the composite samples with different Ag:Cu molar ratios.

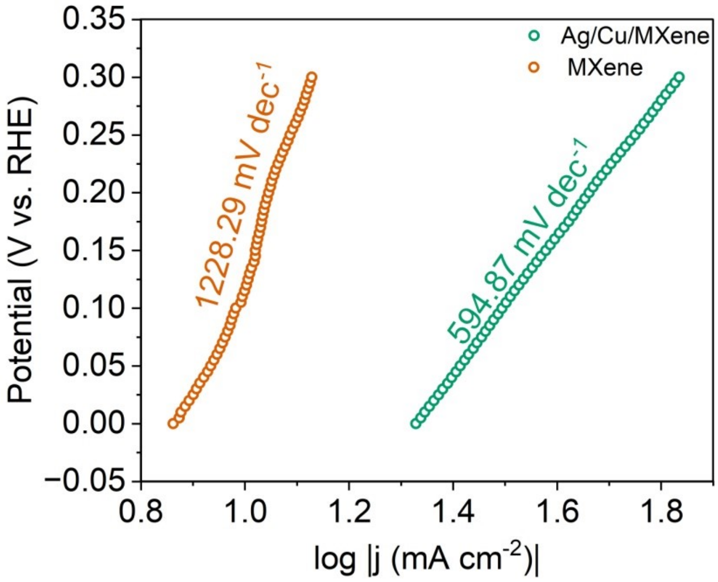

Fig. S6. Tafel slope of Ag/Cu/MXene and MXene samples in NO_3RR.

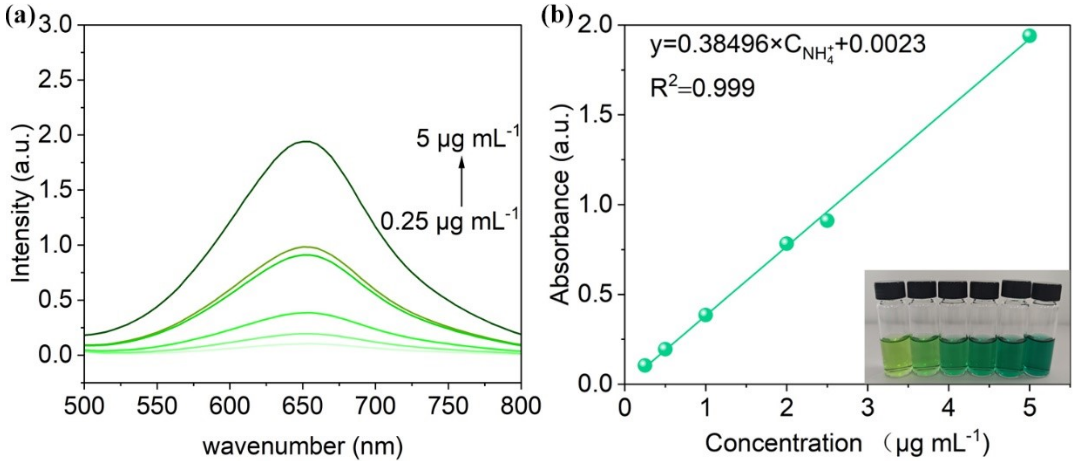

Fig. S7. (a) UV-Vis absorption curves of indophenol assays with different concentrations of NH_4^+ and (b) calibration curve used for the estimation of NH_4^+.

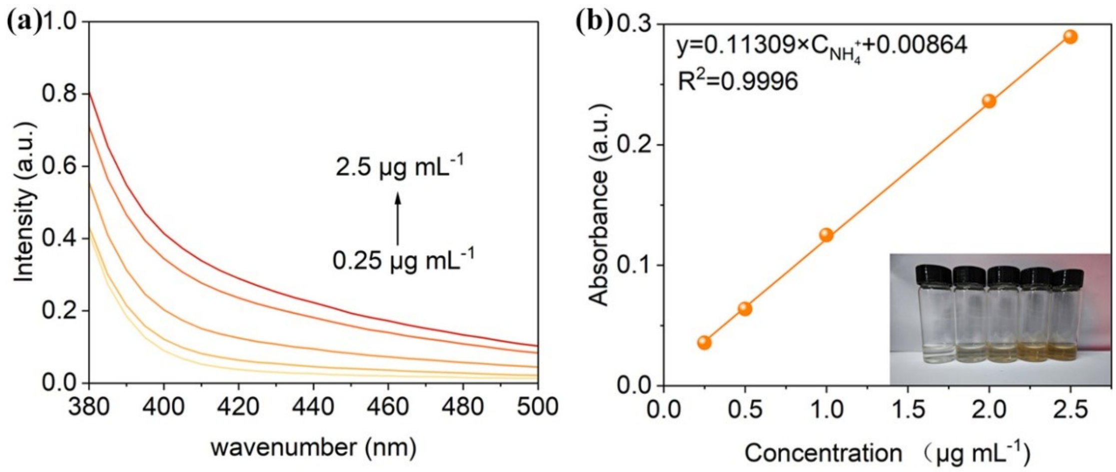

Fig. S8. (a) UV-Vis absorption spectra based on spectrophotometry of Nessler reagent and (b) NH_4^+ concentration-absorbance curve at 420 nm with a series of standard concentrations of NH_4^+ solutions.

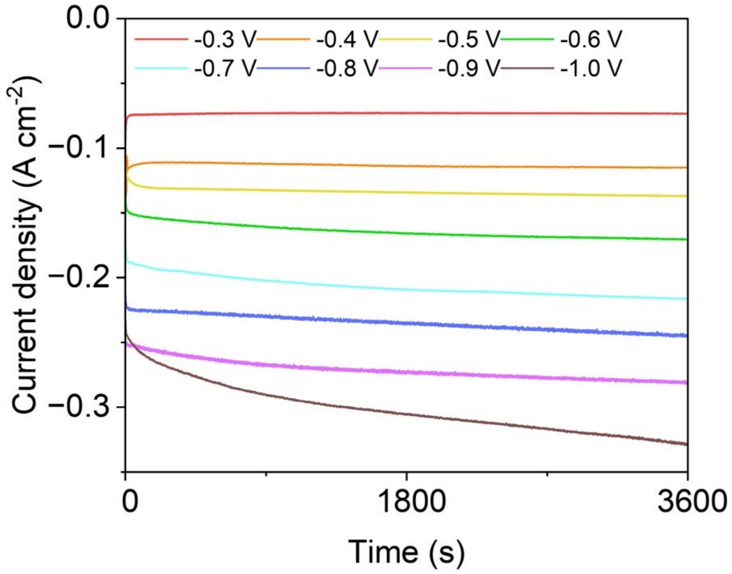

Fig. S9. Potential dependent *I-t* curves of Ag/Cu/MXene composite sample in NO_3RR.

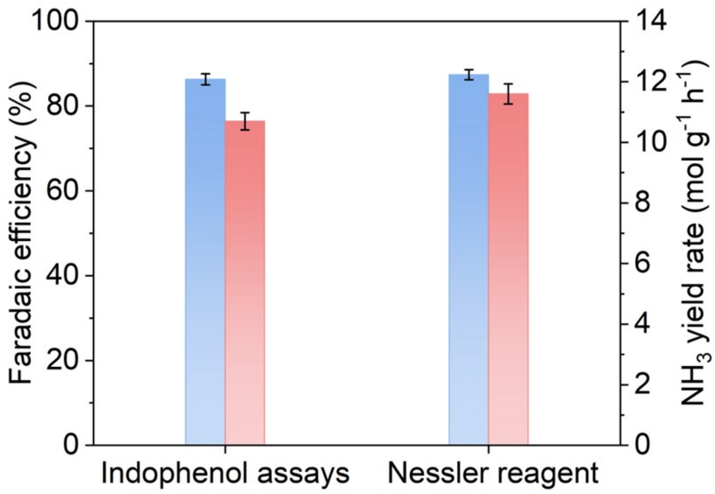

Fig. S10. The comparison of NH_3 yield rates and NH_3 FEs for Ag/Cu/MXene at −1.0 V quantified through indophenol assays method and Nessler reagent method, respectively.

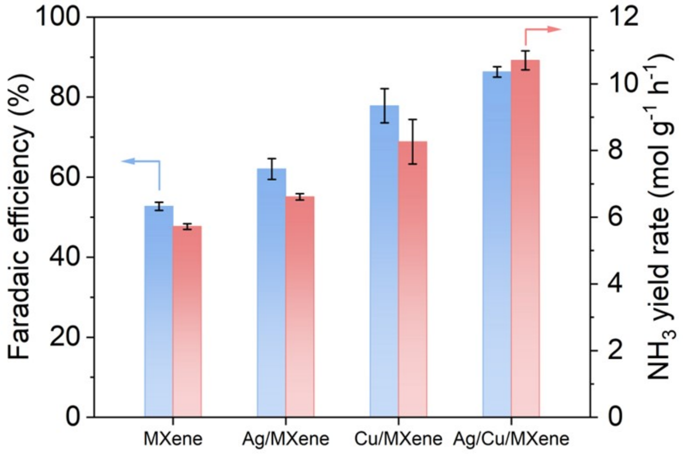

Fig. S11. NH_3 yield rates and NH_3 FEs of MXene, Ag/MXene, Cu/MXene and Ag/Cu/MXene at −1.0 V.

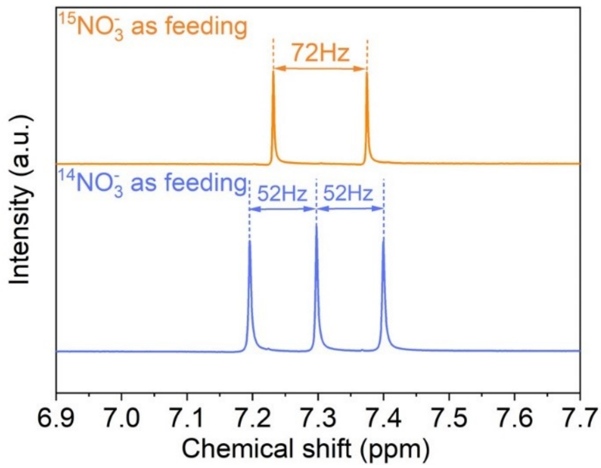

Fig. S12. ^{1}H-NMR spectra of the electrolytes operated in $^{14}NO_3^-$ or $^{15}NO_3^-$ solutions using Ag/Cu/MXene composite sample as a catalyst.

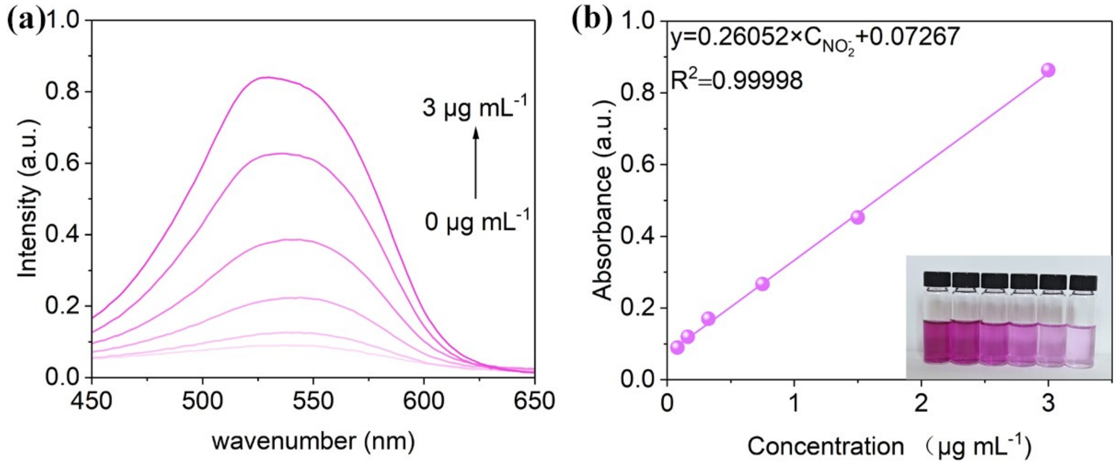

Fig. S13. (a) UV-Vis curves of Griess's regent with varied concentrations of NO_2^- at 100 °C for 15 min. (b) Calibration curve used for the estimation of NO_2^-.

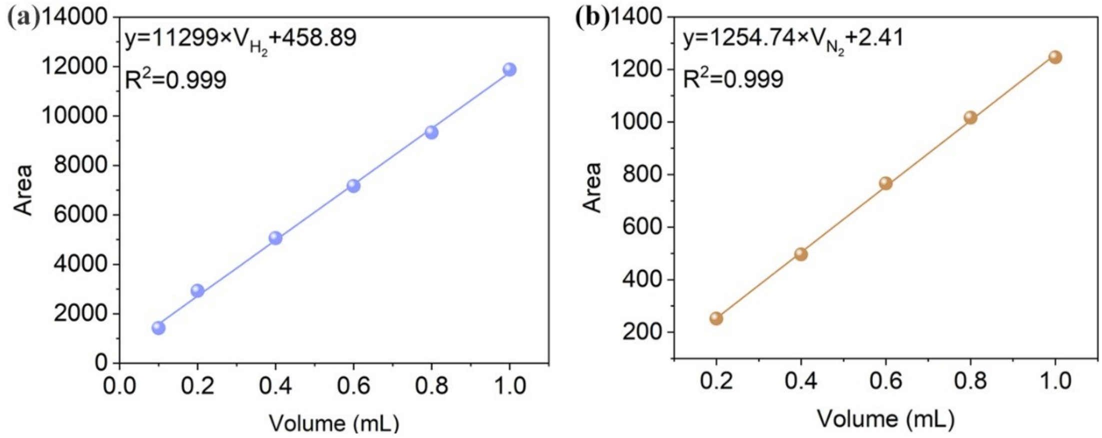

Fig. S14. Working curves for the estimation of (a) H_2 and (b) N_2.

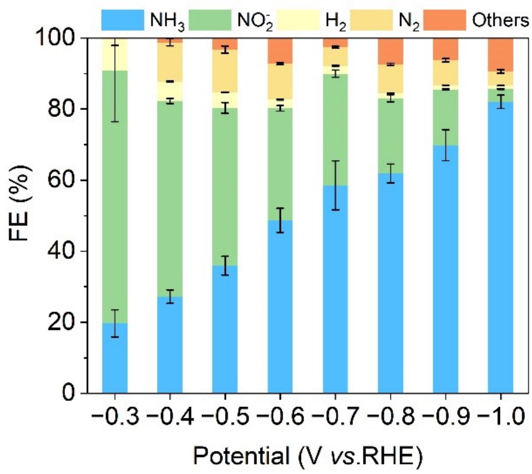

Fig. S15. The FEs of the possible by-products in NO_3RR for Ag/Cu/MXene composite sample.

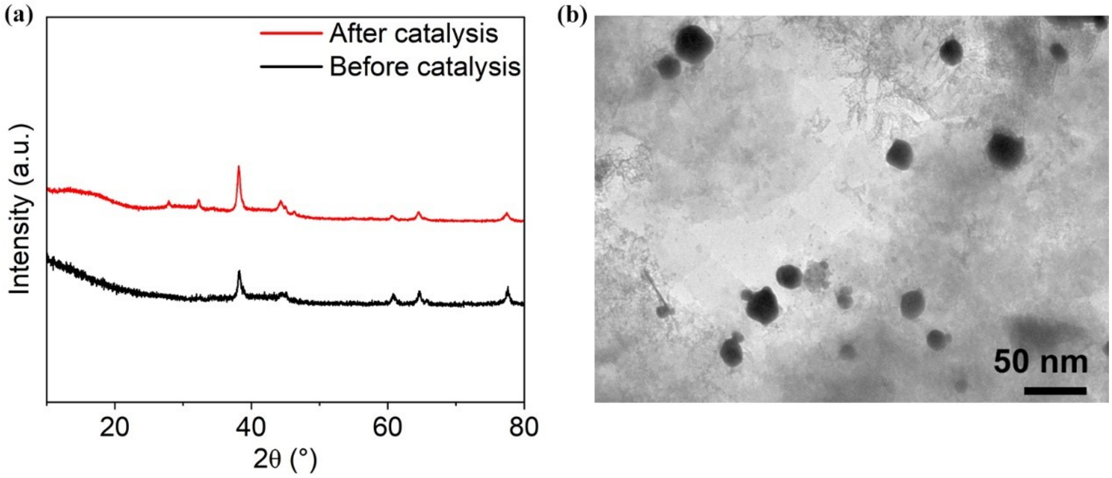

Fig. S16. (a) XRD patterns and (b) TEM image of Ag/Cu/MXene composite sample after catalysis.

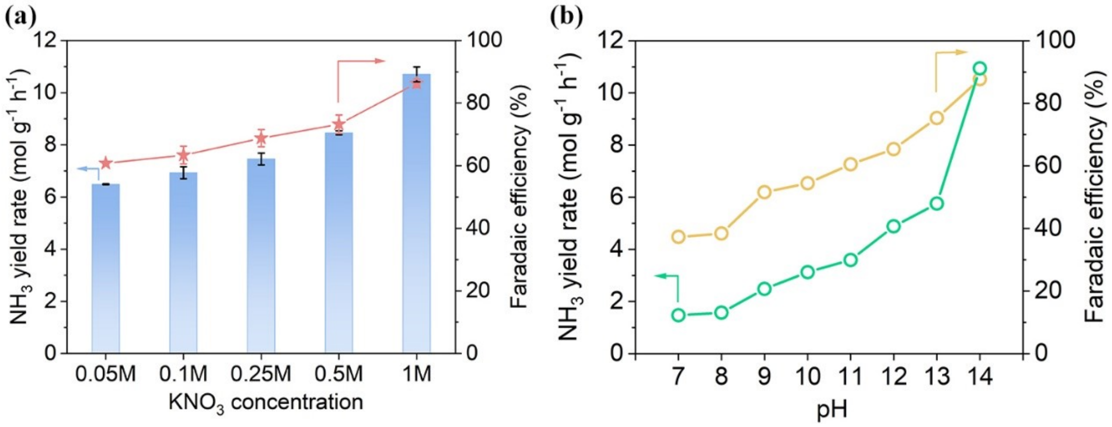

Fig. S17. NH_3 yield rates and FEs of Ag/Cu/MXene composite sample at (a) different concentrations of NO_3^- and (b) pH.

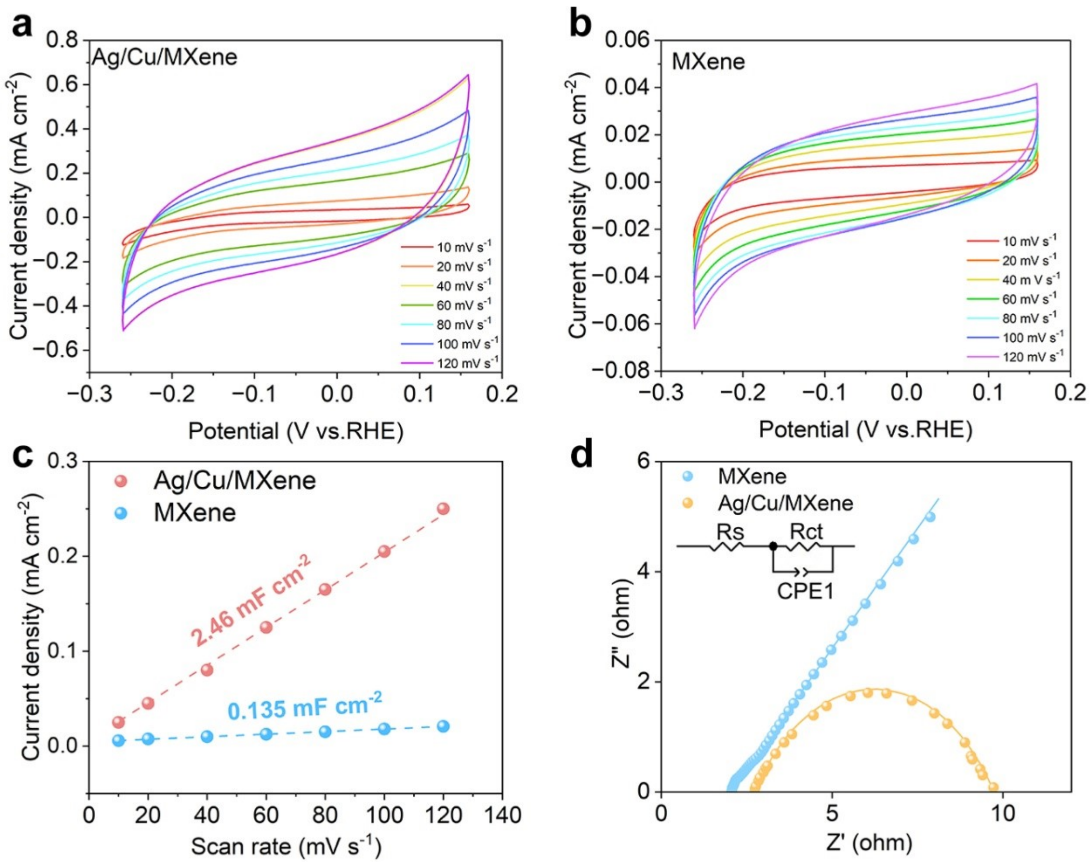

Fig. S18. Cyclic voltammetry curves were recorded at different scanning rates: (a) Ag/Cu/MXene composite sample and (b) MXene. (c) The curve of current density versus scan rates. (d) EIS plots of Ag/Cu/MXene composite sample and MXene.

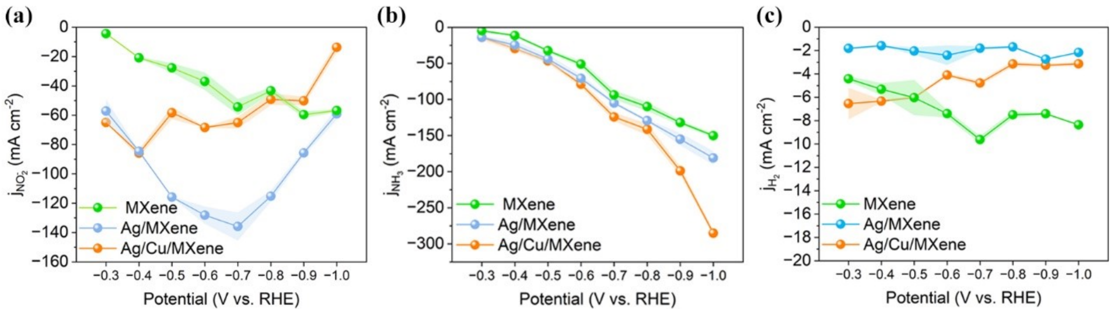

Fig. S19. Partial current densities of Ag/Cu/MXene, Ag/MXene and MXene at different potentials for (a) NO_2^-, (b) NH_3, (c) H_2.

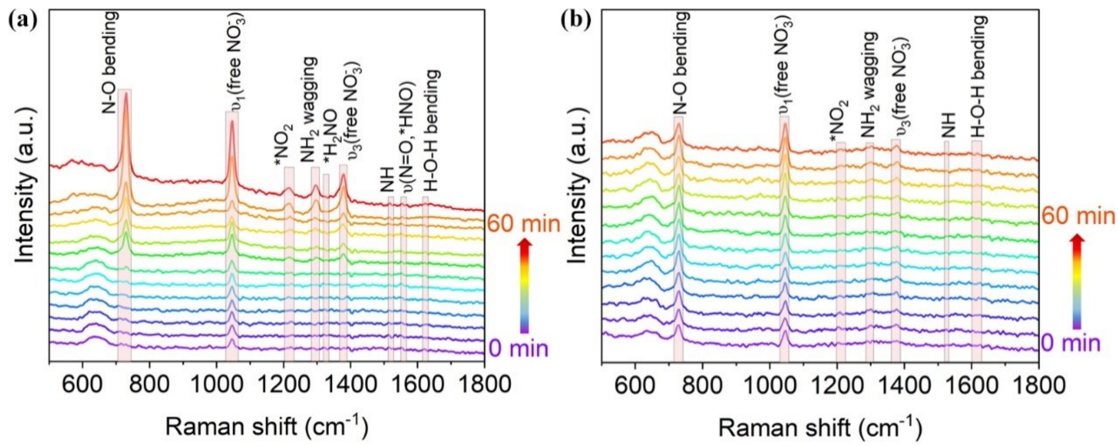

Fig. S20. Time-resolved in situ Raman spectra of (a) Ag/Cu/MXene and (b) MXene.

Table S1. Performance comparison of the Ag/Cu/MXene sample with those recently reported electrocatalysts in NO_3RR.

Catalyst	Electrolyte	NH_3 yield rate	J (mA cm^{-2})	FE (%)	Ref.
Ru-Co CHNWS	1 M NaOH + 1 M $NaNO_3$	8.21 mg cm^{-1} h^{-1}		99	*Chem. Eng. J.* **2024**, *490*, 151883.
Ru-POC	1 M KNO_3	11.2 mg cm^{-1} h^{-1}	~140	96	*CCS Chem.* **2022**, *4*, 3455-3462.
pCuO-10	0.05M KNO_3 + 0.05M H_2SO_4	~0.200 mmol h^{-1} cm^{-2}	~150	~89	*Energy Environ. Sci.* **2021**, *14*, 3588-3598.
Co_3D nanoarray	1 M KOH + 2 M KNO_3	68.4 mg h^{-1} cm^{-2}	1000	86.2	*Nat. Commun.* **2023**, *14*, 1619.
ISAA In−Pd	0.5 M Na_2SO_4 + 0.1 M $NaNO_3$	28.06 mg h^{-1} mg_{pd}^{-1}	800	87.2	*J. Am. Chem. Soc.* **2023**, *145*, 13957-13967.
PdCu-H	0.1 M KOH + 0.01 M KNO_3	9.36 mg h^{-1} $mg_{cat.}^{-1}$		87.3	*Small* **2023**, *19*, 2300794
Plasma treated Cu_2O	50ppm $NaNO_3$-N, 0.5 M Na_2SO_4	0.0825 mmol h^{-1} mg^{-1}	30	89.54	*Appl. Catal. B Environ.* **2022**, *305*, 121021.
Rh@Cu-0.6%	0.1 M Na_2SO_4 + 0.1 M $NaNO_3$	21.59 mg h^{-1} cm^{-2}		93	*Angew. Chem. Int. Ed.* **2022**, *61*, 202202556.
Ag/Cu/MXene	**1 M KOH + 1 M KNO_3**	**10.3 mol $g_{cat.}^{-1}$ h^{-1}**	**320**	**87.7**	**This Work**